DETECTING AIR POCKETS FOR ARCHITECTURAL CONCRETE QUALITY ASSESSMENT USING VISUAL SENSING

SUBMITTED: May 2007
REVISED: September 2007
PUBLISHED: April 2008
EDITORS: B. Akinci and C. Anumba

Zhenhua Zhu, Ph.D. Student
Department of Civil and Environmental Engineering, University of Michigan, Ann Arbor, MI. USA;
email: zhzhu@umich.edu

Ioannis Brilakis, Assistant Professor
Department of Civil and Environmental Engineering, University of Michigan, Ann Arbor, MI. USA;
email: brilakis@umich.edu

SUMMARY: *Air pockets, one kind of concrete surface defects, are often created on formed concrete surfaces during concrete construction. Their existence undermines the desired appearance and visual uniformity of architectural concrete. Therefore, measuring the impact of air pockets on the concrete surface in the form of air pockets is vital in assessing the quality of architectural concrete. Traditionally, such measurements are mainly based on in-situ manual inspections, the results of which are subjective and heavily dependent on the inspectors' own criteria and experience. Often, inspectors may make different assessments even when inspecting the same concrete surface. In addition, the need for experienced inspectors costs owners or general contractors more in inspection fees. To alleviate these problems, this paper presents a methodology that can measure air pockets quantitatively and automatically. In order to achieve this goal, a high contrast, scaled image of a concrete surface is acquired from a fixed distance range and then a spot filter is used to accurately detect air pockets with the help of an image pyramid. The properties of air pockets (the number, the size, and the occupation area of air pockets) are subsequently calculated. These properties are used to quantify the impact of air pockets on the architectural concrete surface. The methodology is implemented in a C++ based prototype and tested on a database of concrete surface images. Comparisons with manual tests validated its measuring accuracy. As a result, the methodology presented in this paper can increase the reliability of concrete surface quality assessment.*

KEYWORDS: *Surface defects, Air pockets, Architectural concrete, Image processing*

1 INTRODUCTION

Concrete is one of widely used construction materials and has a long lifespan (PCA, 2006). However, errors are usually made during construction such as adding improper amounts of water to the concrete mix, inadequate consolidation, and improper curing (ODNR, 1999). These construction errors may result in all kinds of visible defects on the concrete surface. Air pockets, small regular or irregular cavities on the surface of the formed concrete usually less than 15 mm in diameter (ACI 201.1R-92 2005), are one of these defects. The existence of air pockets on the concrete surface impairs the normal function of concrete. For example, they may increase the concrete's permeability. Moreover, they easily make an owner feel discontent about the quality of a finished product. For this reason, air pockets are an important factor in assessing the quality of the concrete surface and inspecting a concrete surface for air pockets is especially necessary for architectural concrete surfaces which are expected to have a high degree of visual uniformity.

Currently, the primary inspection method is manual inspection performed by a qualified inspector with a wealth of knowledge and information (ACI 228.2R-98, 2005). This kind of manual inspection is generally the first step in the comprehensive assessment of a concrete structure (Perenchio, 1989). Its results can be used to differentiate the necessity of performing other inspections. If a manual inspection shows no sign of deterioration, any further actions are not necessary to take and the inspection for the next period can then be scheduled (Sitar, 2005). For example, in the case of assessing existing nuclear safety-related concrete structures, ACI 349.3R (2005) pointed

out that when concrete surfaces satisfy the diameter of air pockets less than 20 mm they are generally acceptable without any other assessments.

However, manual inspection heavily relies on an inspector's personal experience and knowledge, since the criteria that are used in evaluating the final product during inspection are always personally interpreted by inspectors based on their experience gained in previous inspection work. This way, the guide to cast-in-place architecture concrete practice (ACI 303R-04, 2005) requires the inspector to have previous experience in inspecting an infrastructure with equivalent complexity and scope. Also, the inspector is encouraged to gain the experience about the quality of the concrete used through observing the manufacturing of pre-bid samples (ACI 303R-04, 2005). Heavy reliance on an inspector's personal experience leads to subjective assessment, which makes inspection results not always reliable (Yu et al. 2007).

Besides the subjective nature of manual inspection, inspection work performed manually also has other limitations. For example, manual inspection is time-consuming, especially if the inspected structure is complex (Bartel, 2001). The requirement of experienced inspectors also poses a big challenge for the construction industry, which is facing the pressing shortage of experienced and highly trained inspection personnel. The need for an experienced inspector costs owners or general contractors more in inspection fees, since fees for experienced inspectors are significant in comparison with fees for less-experienced inspectors.

Aiming to solve these problems, the goal of this paper is to present a methodology that can help inspectors quantitatively and automatically measure the impact of air pockets on the quality of the concrete surface. At first a high contrast, scaled image of the concrete surface is acquired from a fixed distance. Subsequently spot filters are then adopted to locate the position of air pockets. The number of air pockets is counted from filtering the image results and the size of air pockets is approximated based on the size of the filter and the level of the pyramid used. The impact of air pockets on the quality of the concrete surface is finally measured and quantified according to these calculated properties. The results in this paper show that the presented method can accurately detect air pockets with various sizes. Manual test results validated the effectiveness of the methodology.

2 BACKGROUND

Concrete is mostly composed of cement, water and aggregates (PCA, 2007a). Hardened concrete has certain properties that need to be in satisfactory condition: hydration, drying rate, strength, durability, permeability, volume stability and aesthetics (Wilson, 2006). Aesthetics is now gaining importance within the concrete construction industry. For architectural concrete, it is specified by the American Concrete Institute that the surface of the architectural concrete should be aesthetically compatible with minimal color and texture variations and minimal surface defects (ACI 303R-04, 2005). For structural concrete, similarly, the quality of its surface appearance has been raised to an important position due to the ever-increasing use of exposed structural concrete as an architectural building material (PCA, 2007b).

Air pockets are one primary influence affecting the surface quality of concrete. They generally result from the inadequate consolidation of concrete or the incorrect use of vibrators (ACI 309R-96, 2005) (ACI 212.4R-04, 2005). The existence of air pockets undermines concrete's uniform appearance. Inspection of concrete surfaces in terms of air pockets is therefore necessary to guarantee the desired architectural appearance of buildings designed by the architect/engineer.

2.1 Manual inspection

The primary inspection method is manual inspection. A suitable manual inspection approach typically involves: 1) walking through the inspection area; 2) gathering information on the design, construction and ambient conditions of the structure; 3) planning the complete investigation and 4) laying out a control grid for recording observations (ACI 228.2R-98, 2005). After inspection, the surface condition of the finished product is finally evaluated qualitatively (good, satisfactory and poor) for making a condition survey of concrete (ACI 201.1R-92, 2005).

One of the limitations of manual inspection is that assessment results are not always reliable and even prone to errors (Paterson, 1997). An on-site survey conducted by the Federal Highway Administration (FHWA) Non-Destructive Evaluation Center (NDEVC) observed that routine manual inspections were completed with significant variability. 68 percent of the condition ratings varied within one rating point of the average (NDEVC, 2001). In addition, many work hours are needed for inspectors to become familiar with the structure and to

gather necessary information about background, design and construction documents beforehand. It is especially true in assessing large volumes of concrete in a complex project. Moreover, considering the fact that the construction industry is facing a pressing shortage of an experienced and highly skilled inspection workforce, the requirement of experienced inspectors exacerbates this challenge. Prine (1995) pointed out that many experienced inspection personnel were given early retirement and either were not replaced or were replaced by entry level personnel with minimal experience and training. Lastly, owners or general contractors have to pay sizable inspection fees for hiring experienced inspectors, since the compensation of experienced inspectors is significant. The city of Lincoln (2007) in Canada, for example, pays an experienced inspector $30/hr and only about $21/hr for a less-experienced inspector.

2.2 Sensor-based automated inspection

In order to overcome the limitations of manual inspection, sensor-based automated inspection is therefore proposed and investigated to facilitate inspectors to do inspection work. Images are acquired from digital cameras or infrared scanners operated by inspectors personally or by mobile robots. Concrete surface defects (cracks, coating rusts, air pockets etc.) in these images can then be automatically detected through wavelet transform, Fourier transform, filter convolution and other methods. The features of these surface defects, such as the size of cracks, the orientation of cracks, the diameter of air pockets, are extracted from detection results to assess the target that need to be inspected quantitatively.

2.2.1 Infrared Imaging

Infrared imaging is used to detect near surface anomalies by sensing the temperature of the concrete surface. Since anomalies in the concrete result in temperature differences in local areas, these anomalies can be identified through measuring variations in temperature. Due to its ability to detect large surface area in a short period of time, infrared imaging is a successful inspection method (Starnes et al. 2003). Many researchers explored the possibility of using infrared thermography for concrete surface inspection. Halabe et al. (2005) established surface temperature-time curves. These temperature-time curves can be used to detect embedded near surface defects with different types and sizes. Tommy et al (2004) mapped the temperature contours over the surface of the structure so that an appropriate measure of the delamination of external walls and moisture ingress can be provided. Hu et al, (2002) detected the extent of air blisters according to the fact that concrete or cement paste has higher thermal conductivity than air. In their results, the location of air blisters could be identified remotely as far away as 20 m. The limitations of infrared imaging are that infrared scanners are expensive and operators need to be specially trained. Even so, identification results are still easily influenced by environments (ACI 228.2R-98, 2005). For example, clouds slow heat transfer on the concrete surface, while wind and surface moisture reduce surface temperature gradients. In addition, the existence of brush marks, rubber, or oil residues on the surface also affect its final measurement.

2.2.2 Visual Imaging

Visual imaging is used to analyze concrete surface defects from images generally captured by CCD (Charged Couple Device) cameras. The digital camera industry is improving fast; even consumer cameras can now produce images as high as ten-mega-pixel pictures. So, these digital images can provide detailed information regarding the color or gray-scale attributes of large sized concrete surfaces. The presented inspection procedures based on visual imaging are then able to distinguish a flaw from the rest of the surface and moreover determine size, shape, location, and color attributes of the defect.

For detecting cracks, Yu et al (2007) proposed a system for inspecting and measuring cracks in concrete structures. Their measurement error of the system can be below 10%. Tung et al (2006) developed a mobile manipulator imaging system equipped with binocular cameras for the automation of bridge crack inspection. The geometric information about cracks can be retrieved with two parallel CCD cameras and the maximum measurement error was 3.5 mm when the focus of the camera was set at 500 mm. Lecompte (2006) presented an application of using two cameras for the detection of cracks at the surface of a realistically sized concrete beam and revealed the uncertainty on the measured results is +/- 0.07 pixels. Sinha and Fieguth (2006) introduced the development of a statistical filter for the detection of cracks in buried concrete pipes. The proposed method improved experimental results compared to the conventional detection techniques such as Canny's edge detection (Canny, 1986) and Otsu's thresholding (Otsu, 1979). Pynn et al (1999) carried out the identification of cracks off-line in the developed Highways Agency Road Research Information System (HARRIS) to distinguish

the level (high or low) of roads' cracking. Their method was tested in more than 1000 images and its performance show satisfactory results for highway maintenance planning purpose.

To further improve the reliability of crack detection results, Fujita et al (2006) presented image pre-processing for crack detection to remove irregularly illuminated conditions, shading, blemishes and divots in concrete images. Their method was effective for detecting cracks with noisy concrete real images. Abdel-Qader et al (2003) once compared the effectiveness of crack detection based on four edge-detection techniques: fast Haar transform, fast Fourier transform, Sobel, and Canny. It was revealed that the fast Haar transform is the most reliable by testing a sample of 50 concrete bridge images. Yitzhaky and Peli (2003) proposed a method of selecting edge detection threshold which could automatically select appropriate thresholds for edge detection. Based on this method, an automated procedure for detecting cracks through edge analysis of images was proposed by Hutchinson and Chen (2006) so that cracks along concrete members could be located with minimum human intervention.

In addition to cracks, coating rusts can also be detected and assessed. Lee et al (2005) proposed and evaluated several rust recognition methods in different environmental conditions. These proposed methods are divided into two categories: artificial intelligence based and statistical analysis based. Lee et al (2006) then developed an automated processor to determine whether rust defects exist in a given digital image by processing its digital color information. In their proposed method, it was found that three variables (MEAN in red, DIFF in green and DIFF in blue) had a significant impact in recognizing the existence of bridge coating rust defects.

Most of current existing surface detection methods cannot be applied directly in detecting air pockets, since they do not consider the distinct characteristics of air pockets. For this reason, Suwwanakarn et al (2007) proposed three circular filters to detect air pockets on the surface of concrete. One filter with a large size (11x11) is used to detect large air pockets while the other two filters with a smaller size (5x5) were used to detect small air pockets. The fixed sized filters can guarantee detection results with high precision (the number of air pockets correctly detected over the number of air pockets detected), since high response from filtering an image is always expected where the air pocket exists and its size is similar to the size of the filter. The utilization of the fixed sized filters created a major limitation; only air pockets with the same size as the filters' can be accurately detected. Air pockets with a different size than the sizes of the fixed sized filters cannot be recognized, as shown in Figure 1(a). So, the recall ratio (the number of air pockets detected over the real air pockets on the surface) is low.

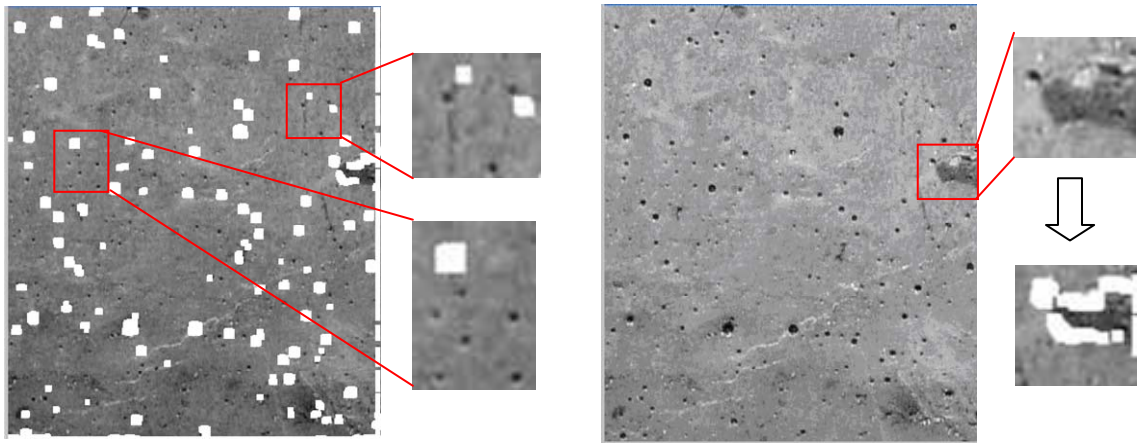

(a) *(b)*

Figure 1: Detecting air pockets: (a) undetected air pockets using one filter with the fixed size and (b) faked air pockets detected around the boundary of other concrete surface defects (Suwwanakarn et al 2007)

In addition, air pocket detection results using the method presented by Suwwanakarn et al (2007) are easily influenced in places where the boundary of other concrete surface defects exists. From Fig. 1(b), it is seen that false air pockets are detected along the edges of the concrete spalling with abruptly changing intensity values. Moreover, applying different filters also brings inconvenience to users. Generally, for one filter, a threshold is given for defining high responses (shown as white regions in Fig. 1(a)) in its convolving result with an image. This threshold is related to the detection results of air pockets. For example, Suwwanakarn et al (2007) gave a

high response threshold. The larger the value of the threshold is, the more air pockets that are detected. No matter what their relationship is, the threshold is specific to the filter, since different filters have different convolving results even within the same image. So, if different filters are applied, users have to specify the threshold for each filter.

3 OVERVIEW OF THE APPROACH

For the sake of overcoming limitations of the method presented by Suwwanakarn et al (2007), a new approach is proposed here. The whole approach is mainly divided into four steps, as illustrated in Fig. 2. Before detecting air pockets, every image has to be initially adjusted to reduce image noise, since images taken with digital cameras always pick up noise and the existence of noise compromises the level of details in digital photos. Salt and pepper noise is a form of noise typically seen on these images. This type of noise only affects a small number of image pixels and represents itself as randomly occurring white and black. Based on this characteristic, the median filter is adopted here. The median filter is a non-linear digital filtering technique and good at removing noise with high spatial frequency from an image (Gregory, 2005). Moreover the median filter does not create new unrealistic pixel values. For this reason, the medial filter can preserve image details, such as causing relatively little blurring of sharp edges in the image (Zou and Dunsmuir, 1997). Examples have been shown that the median filter around 3x3 in size can reduce noise at the expense of a slight degradation in image quality (HIPR, 2000). The result of removing noise with the median filter is illustrated in Fig. 3. After removing noise in the image, the spot filter and the pyramid are applied to locate potential air pockets. Then, properties of air pockets, such as the number, the size and the total area of air pockets are calculated. The visual impact of air pockets to the quality of the concrete surface is produced quantitatively based on these properties.

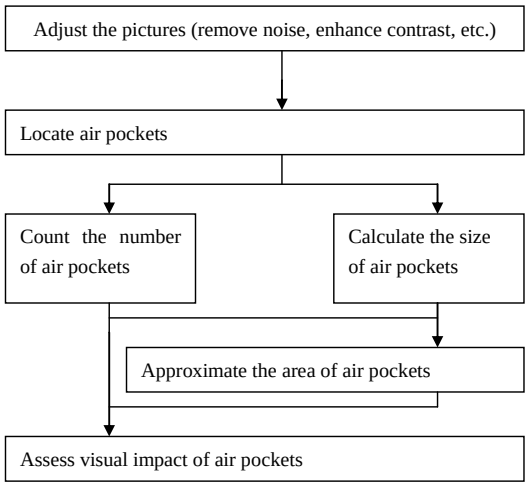

Figure 2: Overview of the approach

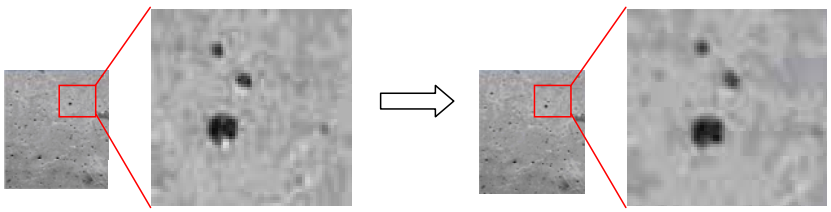

Figure 3: Removing noise with the median filter

4 AIR POCKETS-BASED CONCRETE SURFACE ASSESSMENT

4.1 Air pocket detection filter

To identify air pockets in the image, the unique characteristic of the air pocket had to be considered at first. Usually, the shape of an air pocket on a concrete surface looks like a spot with the inverse intensity value. The intensity value of the air pocket in the image is changing from the dark at the center of the air pocket to the bright at the air pocket's perimeter, until having the same intensity as concrete as shown in Fig. 4.

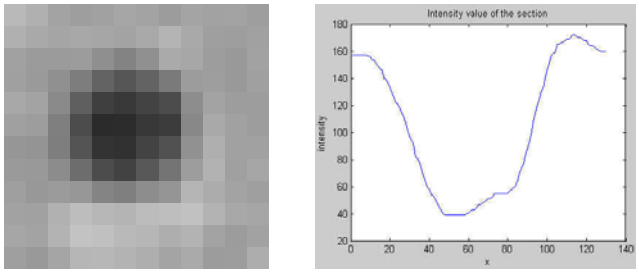

(a) *(b)*

Figure 4: One air pocket: (a) One air pocket in gray-scale image and (b) its intensity value of one section

According to this characteristic of the air pocket in the image, two texture filters that measure spottiness of an image are used as candidate detection filters (Malik and Perona, 1990). Specifically, the first spot filter is formed with a weighted sum of three concentric, symmetric Gaussian filters with weights 1, -2, and 1, and corresponding sigmas 0.62, 1 and 1.6, while the other one is given by a weighted sum of two concentric symmetric Gaussians, with weights 1 and -1, and corresponding sigmas 0.71 and 1.14. Their 3D shapes are illustrated in Figure 5.

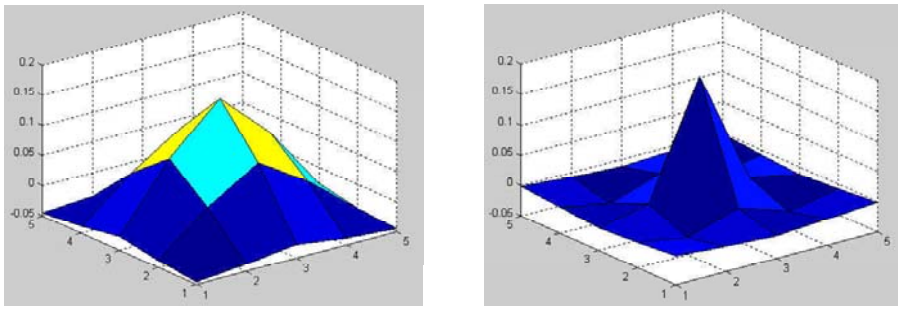

(a) *(b)*

Figure 5: Two kinds of spot filters: (a) the filter composed with three Gaussian filters and (b) the filter composed with two Gaussian filters

When both of two spot filters are applied into images composed of all kinds of air pockets, response values of images to these two filters is retrieved. One example is shown in Fig. 6, where Fig. 6(a) is the image taken by a camera and the response values of the image to these two spot filters are illustrated separately in Fig. 6(b) and 6(c). White regions in these two figures indicate that the tested image has strong responses to the applied filter in these places. It is found that those places which had high response values "happened" to be where air pockets existed. This way, air pockets on the concrete surface can be located through finding high response values in images like Fig. 6(b) and 6(c).

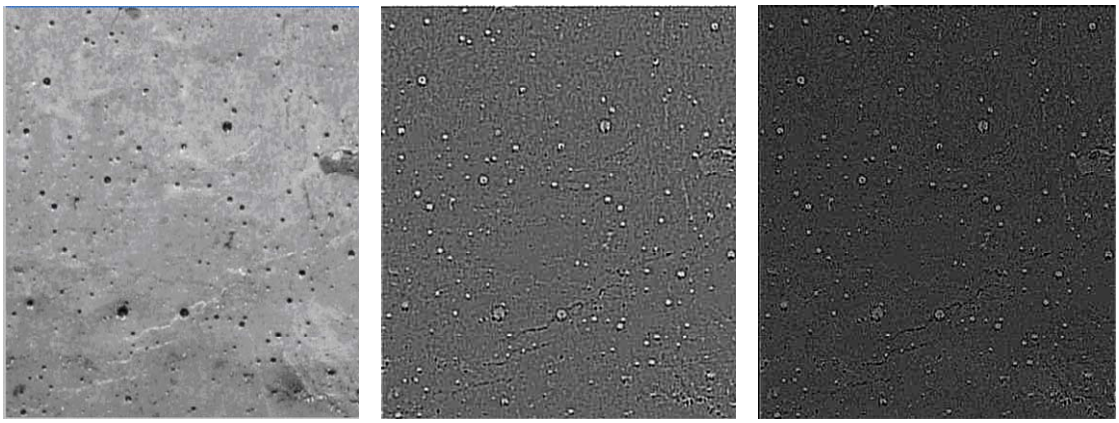

(a) *(b)* *(c)*

Figure 6: Response values of convolving filters; (a) Original image; (b) Response values to the first filter and (c) Response values to the second filter

4.2 The pyramid of an image

If just one filter is applied directly into the image, only air pockets, having the similar size with the filter, can be accurately detected and represented, as mentioned before. Air pockets having the dissimilar size with the filter on the concrete surface cannot be detected and represented accurately. For example, one small actual air pocket is represented by a big detection air pocket (Fig. 7(a)) or by two, three or even four small detection air pockets (Fig. 7(b)). These errors would lead to approximating the size of air pockets incorrectly. Moreover, it would lower down the filter's detection precision and recall ratio, since faked air pockets are introduced in detection results.

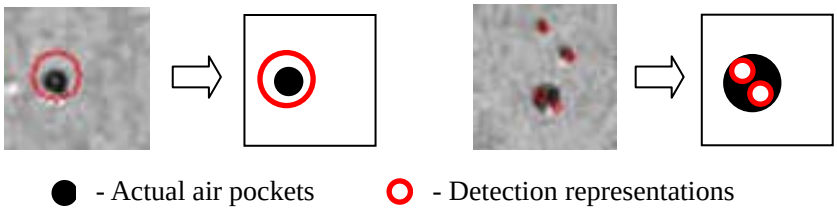

(a) *(b)*

Figure 7: Two kinds of detection failure; (a) failure to detect small air pockets and (b) failure to represent big air pockets

In order to overcome this limitation, the pyramid of an image is introduced. The pyramid is a hierarchy of artificially created images. One example is shown in Fig. 8. In each level of the pyramid, an original image is reduced to a certain percentage in size. It has been already mentioned that the filter can only correctly detect air pockets having the similar size. When the size of an original image is reduced, the size of air pockets on this image is also reduced similarly. So, air pockets whose size is similar to the size of the filter in the original image cannot be detected by the filter any more if the image is reduced enough. As for air pockets whose size is larger than the size of the filter in the original image, they had the similar size as the filter and can be successfully detected, if an appropriate reduction percentage is selected. This way, both small and large air pockets can be detected just with one filter by traversing each level of the pyramid. This point is illustrated in Figure 9.

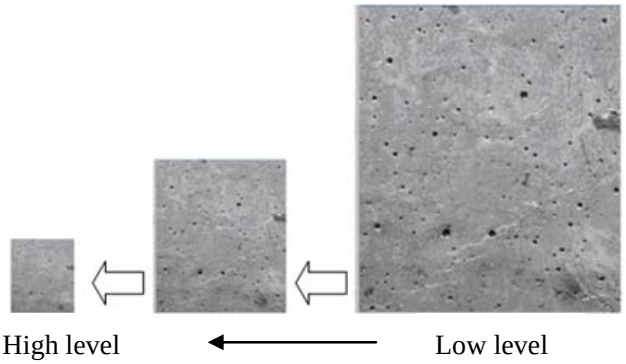

Figure 8: An image pyramid example with three levels

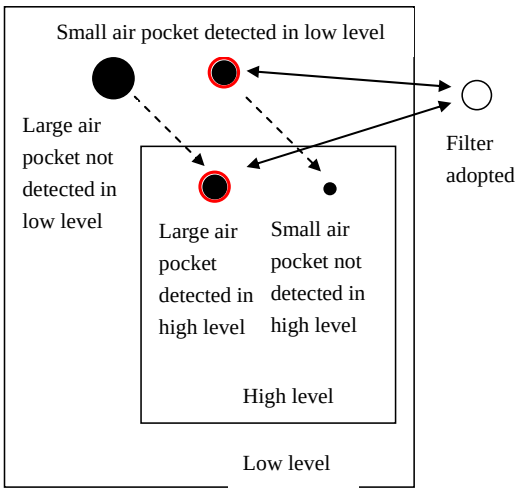

Figure 9: Detecting air pockets using an image pyramid

4.3 Visual impact of air pockets

When applying the filter into the pyramid, high responses in each level of the pyramid are expected. This way, the position of air pockets on the concrete surface can be automatically located by finding the position of these high responses. The number of air pockets on the concrete surface can be calculated by automatically counting the number of these high responses in each level of the pyramid. Also, the size of air pockets detected in one level of the pyramid can be calculated through dividing the size of the filter by the reduction percentage this level adopted. When the number and the size of air pockets are known, the total area of air pockets occupied on the concrete surface can then be deduced as follows. At first the area of air pockets detected in each level of the pyramid is calculated through multiplying the number of air pockets by the size of the size of air pockets. Then the total actual area of air pockets occupied on the concrete surface is obtained by simply adding these air pocket areas in levels.

For the sake of assessing the quality of concrete surface, two visual impact ratios are further calculated. The first one is the percentage of concrete surface that is covered by air pockets over the total area of the concrete surface. The other ratio is calculated by dividing the percentage of concrete surface covered by air pockets with the number of air pockets on the surface. Both of these two ratios are utilized to measure the impact of air pockets on the concrete surface. When the first ratio is small, it means that the area of air pockets on the concrete surface is covered a little. When the first ratio is fixed, if the second ratio is small, it means the number of air pockets on the concrete surface is large compared to the surface they occupy. The number of air pockets visible from a distance is insignificant in this case. When this ratio is large, it means that the number of air pockets on the concrete surface is small compared to the surface they occupy. So, the number of air pockets visible from a

distance is significant. In one word, the smaller both of these two ratios are, the higher the quality of the surface.

5 IMPLEMENTATION AND RESULTS

5.1 Implementation

The prototype for detecting air pockets on the concrete surface is written in Visual C++. The prototype also used OpenCV (Intel® Open Source Computer Vision Library) as its main image processing toolbox. OpenCV is a collection of C functions and C++ classes that implement many popular algorithms about image processing and computer vision (Intel, 2007). It is free for both non-commercial and commercial use.

A series of screenshots (Fig. 10 (a), (b), (c) and (d)) show the major process of detecting air pockets on the concrete surface image using the prototype developed in this paper. Among them, Fig. 10(a) shows the main interface of the prototype, where the image can be loaded. After that, users are allowed to select the concrete surface that need to be inspected, as shown in Fig. 10(b). From the menu, air pockets detection is selected (Fig. 10(c)) and detection results for air pockets in the selected surface are then displayed in Fig. 10(d).

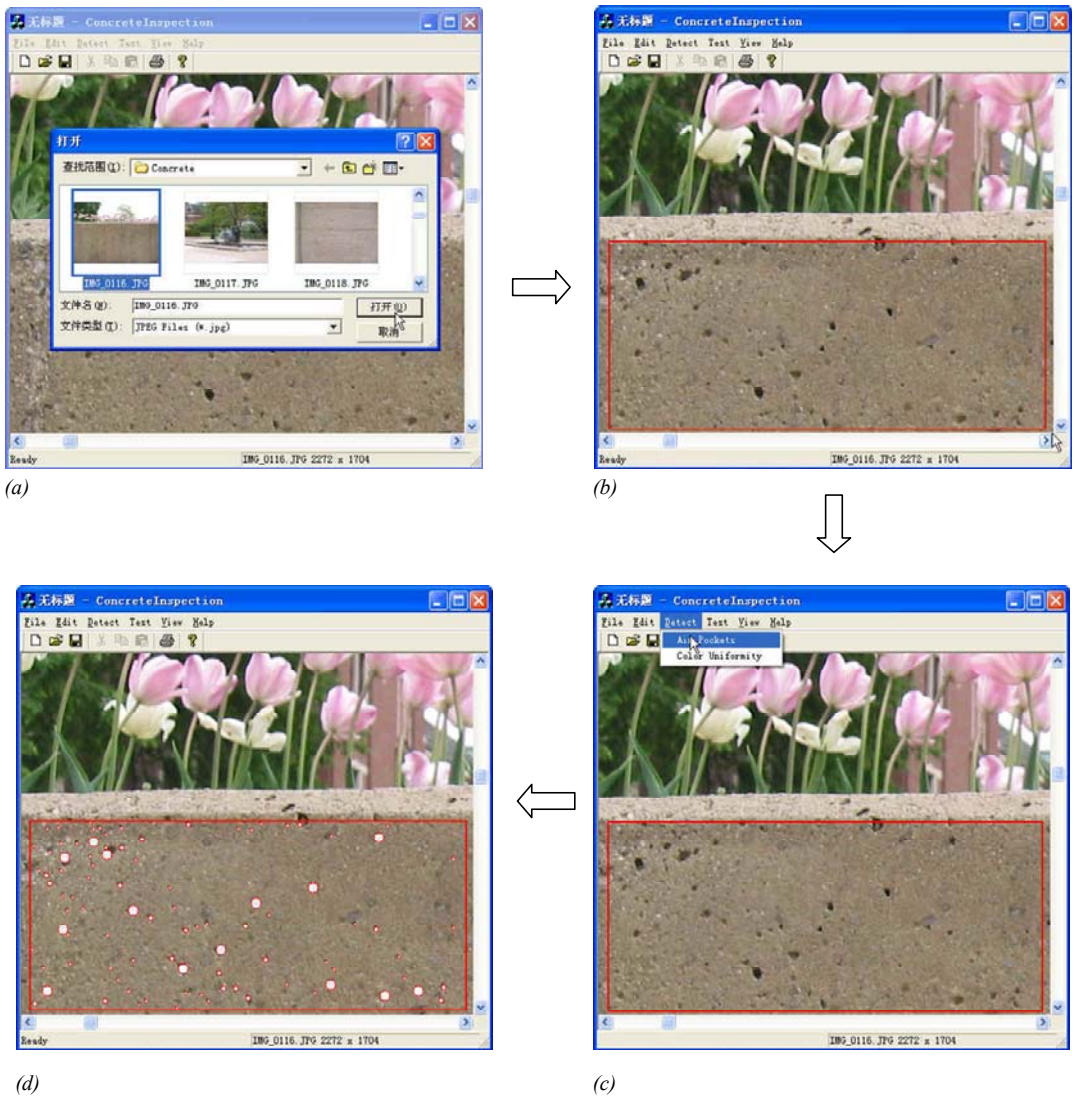

(a) *(b)* *(c)* *(d)*

Figure 10: Process of detecting air pockets with the prototype; (a) open image file; (b) select detected region; (c) select air pockets detection and (d) display detection results

5.2 Results

5.2.1 Detection precision and recall

Detection precision is the percentage that the number of air pockets correctly detected over the number of air pockets detected, while detection recall is the percentage of the number of air pockets correctly detected over the number of actual air pockets on the surface. Both of them are useful for measuring the quality of detection results. High detection precision means most detected air pockets are actual air pockets and high detection recall means most of actual air pockets are correctly detected. Also they can be regarded as criteria to measure the preferable type of filters adopted. It is known that different types of filters have different response values when the image is filtered, as shown in Fig. 6(b) and Fig. 6(c). So did their detection precision and recall. Fig. 11 shows the difference in the detection precision and recall of both spot filters described in the previous section. Although both of filters can achieve high precision ratios in their detecting results, the recall ratios of these two filters are different. The filter composed with three concentric and symmetric Gaussian filters can retrieve 86% of actual air pockets in the case of the detection precision: 91%. Almost at the same detection precision (92%), the filter composed with two concentric and symmetric Gaussian filters can only retrieve 74% of actual air pockets. So, the spot filter formed with a weighted sum of three concentric, symmetric Gaussian filters with weights 1, -2, and 1 is preferable.

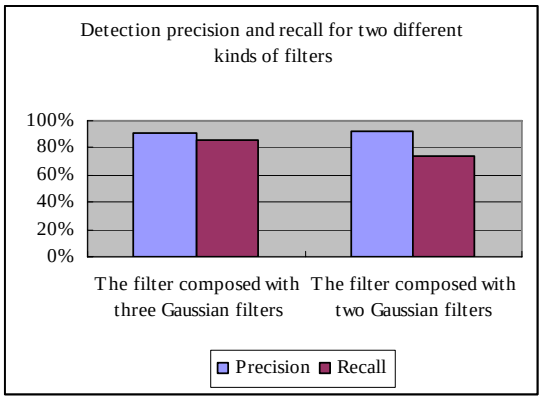

Figure 11: Precision and recall of air pockets detection with two different kinds of filters

In addition to measuring different types of filters, precision and recall can also be used to determine the optimum size of one selected filter. The size of the filter has an important impact on detection results, since the strong response of the air pocket to the filter is guaranteed only when the size of the air pocket is similar to that of the applied filter. Filters with sizes 5x5, 7x7, 9x9 and 11x11 are tested here and their relationship between the filter's size and their precision and recall ratios is illustrated in Fig. 12. From the figure, it is found that the precision of different sized filters increased a bit (91%, 93%, 94% and 93%)) but are still maintained at the same level, while the recall ratio is decreasing when the size of the filter increases from 5x5 to 11x11 (83%, 66%, 53% and 43%). It is true since the filter with small size can not only detect small air pockets but also large ones in the aid of an image pyramid, while the filter with large size can detect large air pockets only.

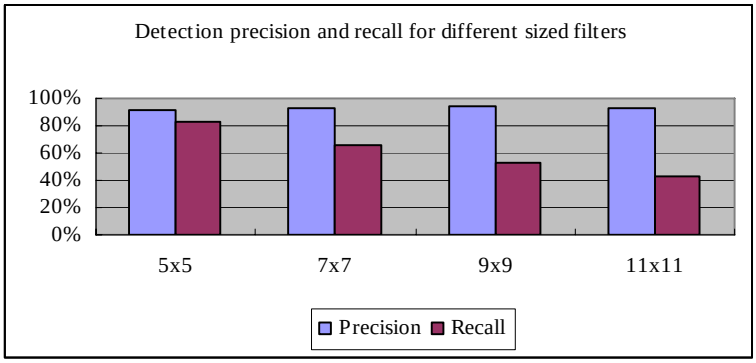

Figure 12: Precision and recall of air pockets detection with different sized filters

5.2.2 Detected air pockets distribution

Besides detection precision and recall ratios, detected air pockets distribution according to their size is also tested to measure the degree of approximating actual air pockets on the concrete surface in size with the method presented in this paper. To do so, an air pocket distribution table to classify actual air pockets based on their diameters is manually given. Air pockets on a concrete surface are classified with the table so that the distribution of actual air pockets in the form of the number of air pockets is known. Table 1 shows the classification result of one concrete surface image (Fig. 6(a)). Its corresponding distribution of air pockets on the surface is shown in Fig. 13. The diameter of actual air pockets in the image is measured in pixels for the convenience of comparison between images.

Table 1: Classification of air pockets according to their diameters

	The diameter of air pockets (X)										
	3>X	*4>X≥3*	*5>X≥4*	*6>X≥5*	*7>X≥6*	*8>X≥7*	*9>X≥8*	*10>X≥9*	*11>X≥10*	*12>X≥11*	*X≥12*
Number of air pockets	*39*	*59*	*34*	*24*	*22*	*3*	*2*	*1*	*1*	*1*	*1*

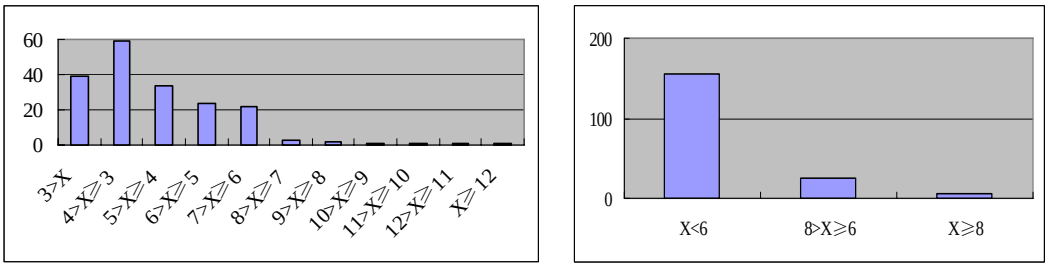

(a) *(b)*

Figure 13: Distribution of air pockets; (a) distribution in each category and (b) the number of actual air pockets in three levels

Table 2 illustrates the effect of reducing the size of an original concrete surface image (Fig. 6(a)) on the detection results of the selected filter. The size of the image (Fig. 6(a)) is reduced to the percentage shown in Table 2, and the selected spot filter is directly applied. The air pockets detected are then recorded. In order to compare the detection ability of the selected filter on different sized air pockets, those detected air pockets are classified according to their diameter in the original image (shown in Table 2(a)). Then, the recall ratio of detected air pockets in each category is calculated (shown in Table 2(b)). From the Table 2, it is seen that the ability of the filter in detecting air pockets can only be achieved when the size of air pockets is close to the size of adopted filter. For example, the adopted 5x5 spot filter can detect only 86% air pockets with the size between 6 and 7, but can detect 91% air pockets with the size range between 4 and 5 in the original image. This point can also be illustrated in the other way. Still take air pockets with the size between 6 and 7 as an example. When the image size is reduced, the number of the detected air pockets in this size range (between 6 and 7) is increased. This is because the reduction of the size of the image scales a large air pocket to be a small one. The maximum detection ability for those air pockets is achieved when the image size is reduced to 70%. At that time, the size of air pockets is actually scaled to approximately between 4.2 (6*0.7) and 4.9 (7*0.7), which is very close to the size range between 4 and 5 and the size of adopted filter (5x5).

Table 2: Detection results when applying a filter in reduced sized images: (a) the number air pockets detected in each category and (b) the detection recall (the detected number of air pockets/the actual number of air pockets) in each category

		The diameter of air pockets (X)										
		3>X	*4>X≥3*	*5>X≥4*	*6>X≥5*	*7>X≥6*	*8>X≥7*	*9>X≥8*	*10>X≥9*	*11>X≥10*	*12>X≥11*	*X≥12*
The percentage of the size of the original concrete surface image	*100%*	*24*	*48*	*31*	*21*	*19*	*0*	*0*	*0*	*0*	*0*	*0*
	90%	*19*	*37*	*30*	*23*	*20*	*0*	*0*	*0*	*0*	*0*	*0*
	80%	*12*	*36*	*29*	*24*	*21*	*0*	*0*	*0*	*0*	*0*	*0*
	70%	*9*	*18*	*27*	*22*	*22*	*1*	*0*	*0*	*0*	*0*	*0*
	60%	*1*	*8*	*17*	*20*	*19*	*2*	*0*	*0*	*0*	*0*	*0*
	50%	*1*	*5*	*12*	*19*	*19*	*3*	*2*	*0*	*0*	*0*	*0*
	40%	*1*	*1*	*1*	*9*	*19*	*3*	*2*	*1*	*1*	*1*	*1*
	30%	*1*	*1*	*2*	*5*	*9*	*1*	*2*	*1*	*1*	*1*	*1*
	20%	*0*	*0*	*0*	*1*	*2*	*1*	*2*	*0*	*1*	*1*	*1*
	10%	*0*	*0*	*0*	*0*	*1*	*0*	*0*	*0*	*0*	*1*	*1*

(a)

		The diameter of air pockets (X)										
		3>X	*4>X≥3*	*5>X≥4*	*6>X≥5*	*7>X≥6*	*8>X≥7*	*9>X≥8*	*10>X≥9*	*11>X≥10*	*12>X≥11*	*X≥12*
The percentage of the size of the original concrete surface image	*100%*	*62%*	*81%*	*91%*	*88%*	*86%*	*0%*	*0%*	*0%*	*0%*	*0%*	*0%*
	90%	*49%*	*63%*	*88%*	*96%*	*91%*	*0%*	*0%*	*0%*	*0%*	*0%*	*0%*
	80%	*31%*	*61%*	*85%*	*100%*	*95%*	*0%*	*0%*	*0%*	*0%*	*0%*	*0%*
	70%	*23%*	*31%*	*79%*	*92%*	*100%*	*33%*	*0%*	*0%*	*0%*	*0%*	*0%*
	60%	*3%*	*14%*	*50%*	*83%*	*86%*	*67%*	*0%*	*0%*	*0%*	*0%*	*0%*
	50%	*3%*	*8%*	*35%*	*79%*	*86%*	*100%*	*100%*	*0%*	*0%*	*0%*	*0%*
	40%	*3%*	*2%*	*3%*	*38%*	*86%*	*100%*	*100%*	*100%*	*100%*	*100%*	*100%*
	30%	*3%*	*2%*	*6%*	*21%*	*41%*	*33%*	*100%*	*100%*	*100%*	*100%*	*100%*
	20%	*0%*	*0%*	*0%*	*4%*	*9%*	*33%*	*100%*	*0%*	*100%*	*100%*	*100%*
	10%	*0%*	*0%*	*0%*	*0%*	*5%*	*0%*	*0%*	*0%*	*0%*	*100%*	*100%*

(b)

When the detection recall ratio of the filter in each air pocket category is retrieved (Table 2(b)), the detection ability of the filter can be measured and depicted as a curve shown in Figure 14. For one image, the filter can detect most air pockets in a certain size range. Take 100% sized image as an example in Figure 16. The filter can mainly detect small air pockets but miss large one. This limitation is solved by adjusting the size of the image. For example, when the size of the image is reduced to 40% of the original image (40% sized image), large air pockets can be detected. However, small air pockets are missed at that time. Thus, images with different size are combined for the filter to detect as many air pockets as possible. Three images are selected here. They are the images with 100%, 70% and 40% of the size of the original image. The detection ability of the filter for each image is shown in Fig. 14. The detection result using these three images is illustrated in Fig. 15, where the detected actual air pockets are represented by red circles. The larger the air pocket, the bigger the red circle. Those detected air pockets are classified into three levels according to the image used for detection. Level 1 is for the air pockets detected on the image with 100% of the size of the original image, while Level 3 is for the air pockets detected on the image with only 40% of the size of the original image. The number of detected air pockets in these three levels is recorded in Fig. 16. Compared with the number of actual air pockets in three levels in Fig. 15(b), the distribution of detected air pockets fits the distribution of actual air pockets closely.

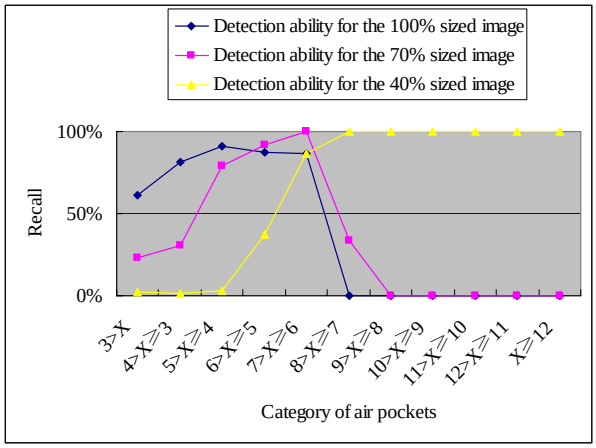

Figure 14: Air pockets detection recall in three images whose sizes are 100%, 70% and 40% of the original image (Figure 6(a))

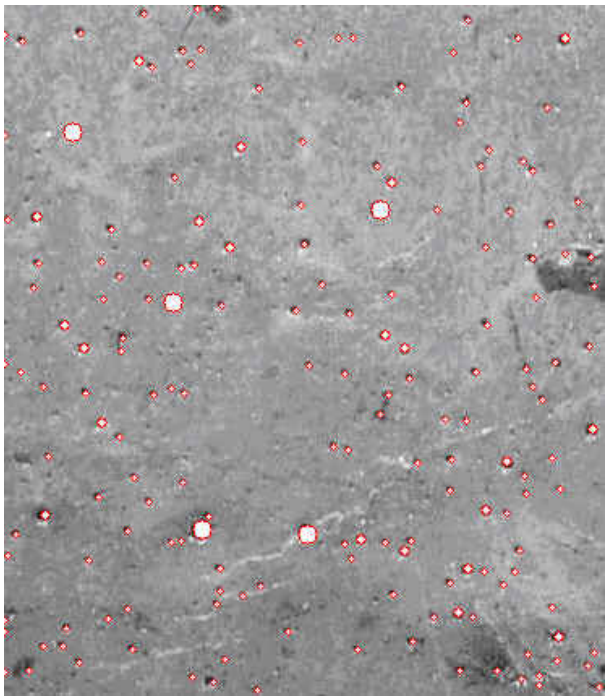

Figure 15: Detection of air pockets through the spot filter and the pyramid

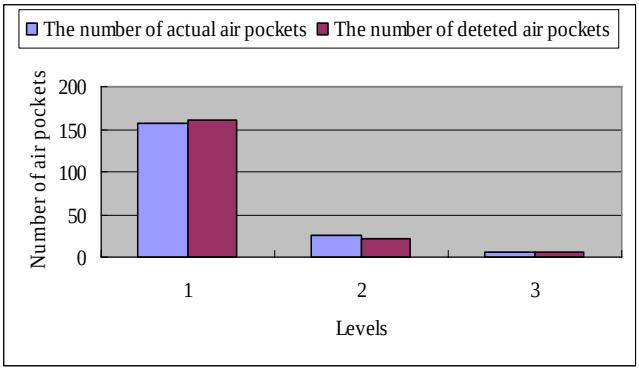

Figure 16: Distribution of detected and actual air pockets

5.2.3 Quality of detection results

A database of concrete surface images is tested in the prototype. One part of test results is shown in Table 3, where results are measured using two ratios (detection precision and detection recall). From Table 3, it is seen that detection precision ranges from 77.4% to 96.8% and the average detection precision is maintained at 91.1% with the standard deviation 5.5%, while detection recall ranges from 77.0% to 92.4% and the average detection recall is maintained at 85.6% with the standard deviation 6.0%. At the same time visual impact ratios are also calculated. Visual impact ratios can be used to measure the quality of concrete surfaces. For example, although both concrete surfaces in image (e) and image (g) are covered with many air pockets (shown in Fig. 17), the quality of concrete surface in image (g) is a bit better than that in image (e), because the concrete surface in image (e) mainly consist of air pockets with a large size while the concrete surface in image (g) mainly consist of air pockets with a small size. Their calculated visual impact ratios also reflect this. Both visual impact ratio 1 and 2 of the concrete surface in image (e) are higher than those of the concrete surface in image (g).

Table 3: Detection precision and recall for 11 images

Image	*Number of Air Pockets Detected*	*Actual Air Pockets*	*Number of Air Pockets Correctly Detected*	*Precision*	*Recall*	*Visual Impact Ratio 1*	*Visual Impact Ratio 2*
(a)	*188*	*190*	*163*	*86.7%*	*85.8%*	*2%*	*0.10‰*
(b)	*132*	*136*	*124*	*93.9%*	*91.2%*	*3%*	*0.21‰*
(c)	*139*	*159*	*123*	*88.5%*	*77.4%*	*3%*	*0.24‰*
(d)	*95*	*106*	*90*	*94.7%*	*84.9%*	*2%*	*0.18‰*
(e)	*93*	*113*	*87*	*93.5%*	*77.0%*	*4%*	*0.42‰*
(f)	*126*	*154*	*122*	*96.8%*	*79.2%*	*3%*	*0.20‰*
(g)	*195*	*226*	*184*	*94.4%*	*81.4%*	*2%*	*0.12‰*
(h)	*31*	*26*	*24*	*77.4%*	*92.3%*	*2%*	*0.82‰*
(i)	*181*	*184*	*170*	*93.9%*	*92.4%*	*6%*	*0.31‰*
(j)	*120*	*118*	*107*	*89.2%*	*90.7%*	*4%*	*0.35‰*
(k)	*173*	*180*	*160*	*92.5%*	*88.9%*	*4%*	*0.21‰*
Average in (a) – (k)				*91.1%*	*85.6%*		
Standard deviation in (a) – (k)				*5.5%*	*6.0%*		

Detection precision - the number of air pockets correctly detected / the number of air pockets detected
Detection recall - the number of air pockets correctly detected over the number of actual air pockets

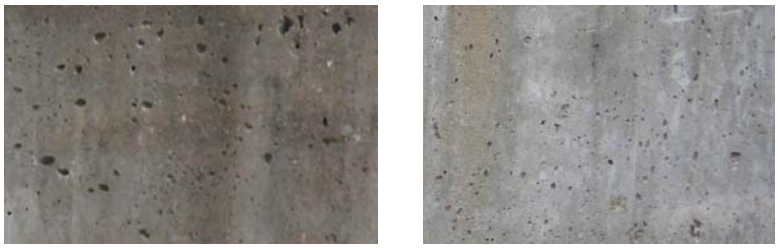

(a) *(b)*

Figure 17: Comparison between image(e) and image(g); (a) image(e) and (b) image(g)

The effectiveness of the method in this paper is also compared with the method presented by Suwwanakarn et al (2007) using the image Fig. 6(a) as an example. Two cases are explored in the method presented by Suwwanakarn et al (2007). The first one is application of 11x11 filter and 5x5 filter type 1 to detect air pockets while the other is application of 11x11 filter and 5x5 filter type 2 to detect air pockets. In the former case, the detection precision (86.0%) almost equals to the detection precision using the method presented in this paper (86.7%), but the corresponding recall (48.4%) is lower than the detection recall using the method presented in this paper (85.8%). In the latter case, both detection precision and recall (69.2% and 38.9%) are lower than the detection precision and recall using the method presented in this paper. Table 4 illustrates this point.

Table 4: Comparison using Figure 6(a) as an example

	The method presented in Suwwanakarn et al (2007)		*The method presented in this paper*
	11x11 filter + 5x5 filter type 1	*11x11 filter + 5x5 filter type 2*	
Number of Actual air pockets	*190*	*190*	*190*
Number of detected air pockets	*107*	*107*	*188*
Number of correctly detected air pockets	*92*	*74*	*163*
Precision	*86.0%*	*69.2%*	*86.7%*
Recall	*48.4%*	*38.9%*	*85.8%*

6 CONCLUSIONS AND FUTURE WORK

Concrete defects appear on the surface of concrete during construction or within a relatively short time after completion. These defects are inevitable within the construction industry. The existence of these concrete effects especially surface defects, such as air pockets, not only impairs the normal function of concrete, but also undermines the visual uniformity of concrete surfaces. Therefore inspecting them is necessary to guarantee the final quality of the project. Currently, manual inspection is widely used; however, manual inspection has its own limitations. For example, it is subjective and therefore not always reliable. In addition, it is time-consuming. The high requirement of the inspector also aggravates the shortage of work force in the construction industry. Automatic inspection can overcome these limitations.

This paper presents an automatic inspection methodology for detecting air pockets on the concrete surface. The methodology consists of four steps. Initially, noise in concrete surface images is removed with the media filter. After that spot filters and image pyramids are applied to locate air pockets on these images according to the circular characteristic of air pockets. For these detected air pockets, the number of air pockets on the concrete surface is calculated by automatically counting the locations that the filter detected. Also, the size of the air pockets is approximated from the size of the filter and the level of the pyramid used. Moreover, the total area of air pockets covered on the surface is calculated through the calculated size of each air pocket. Finally, two visual impact ratios are introduced to measure the surface quality of concrete quantitatively.

Inspectors can measure the quality of the concrete surface in terms of air pockets with the method presented in this paper. Also inspectors can save time in inspecting the quality of the concrete surface and owners will be able to use less experienced, lower cost inspectors for this type of inspection, since only taking pictures of the under-inspection surfaces is needed during the on-site visit. For example, in the City of Lincoln in Canada, this could save the City $9 /hr per inspector. The method is implemented using Microsoft Visual C++. OpenCV is used as the image processing tool developed by Intel. Experiment results in this paper validated the effectiveness of the proposed method.

The quantitative inspection results are objective, but they are difficulty for people without inspection experience to understand. Therefore, future work will establish the relationship between the quantitative inspection results and qualitative surface condition ratings currently applied in ACI documents. Moreover the detection of other surface defects, such as color variation will also be focused on.

ACKNOWLEDGEMENT

Mr. Clark, Phillip A. kindly preformed concrete manual inspection work for this paper and at the same time proofread the paper. The above support is gratefully acknowledged.

REFERENCES

Abdel-Qader I., Abudayyeh O., and Kelly, M. E. (2003), "Analysis of Edge-Detection Techniques for Crack Identification in Bridges", Journal of Computation in Civil Engineering., Volume 17, Issue 4, pp. 255-263

ACI 201.1R-92, (2005) "Guide for Make a Condition Survey of Concrete", ACI Manual of Concrete Practice 2005

ACI 212.4R-04, (2005), "Behavior of Fresh Concrete during Vibration", ACI Manual of Concrete Practice 2005

ACI 228.2R-98, (2005), "Nondestructive Test Methods for Evaluation of Concrete in Structures", ACI Manual of Concrete Practice 2005

ACI 303R-04, (2005), "Guide for Cast-in-Place Architecture Concrete Practice", ACI Manual of Concrete Practice 2005

ACI 309R-96, (2005), "Guide for Consolidation of Concrete", ACI Manual of Concrete Practice 2005

ACI 349.3R, (2005), "Evaluation of Existing Nuclear Safety-Related Concrete Structures", ACI Manual of Concrete Practice 2005

Bartel J., (2001), "A picture of bridge health." NTIAC (Nondestructive Testing Information Analysis Center) Newsletter, 27~1, 1–4.

Canny J.F., (1986), "A computational approach to edge detection", IEEE Trans. Pattern Anal. Mach. Intell. 8 (1986) (6), pp. 679–698

City of Lincoln (Lincoln), (2007), "Construction Inspector I/II", last visit: http://www.ci.lincoln.ca.us/pagedownloads/Construction%20Inspector%20I-II%20web%2002-07.pdf

Federal Highway Administration's Nondestructive Evaluation Validation Center (NDEVC), (2001), "Reliability of Visual Inspection for Highway Bridges, Volume I: Final Report and, Volume II: Appendices", Publication Nos. FHWA-RD-01-020 and -021, last visit: http://www.tfhrc.gov/hnr20/nde/01105.pdf

Fujia Y., Yoshihiro M., and Yoshihiko H. (2006), "A Method for Crack Detection on a Concrete Structure", 18th International Conference on Pattern Recognition (ICPR'06) pp. 901-904

Gregory N.G., (2005), "Noise Characterization of Consumer Digital Camera", last visit: http://scien.stanford.edu/class/psych221/projects/05/gregng/index.html

Halabe UB., Vasudevan A., GangaRao HVS., Klinkhachorn P. and Lonkar G., (2005), "Subsurface Defect Detection in FRP Composites Using Infrared Thermography", American Institute of Physics Conference Proceedings, Vol 760 pp. 1477-1484.

Hypermedia Image Processing Reference (HIPR), (2000), "Median filter", last visit: http://homepages.inf.ed.ac.uk/rbf/HIPR2/median.htm

Hu C.W., Shih J.K.C, Delpak R., Tann D.B., (2002), "Detection of air blisters and crack propagation in FRP strengthened concrete elements using infrared thermograph",

Hutchinson T.C. and Chen ZQ., (2006), "Improved Image Analysis for Evaluating Concrete Damage", Journal of Computing. in Civil Engineering, Volume 20, Issue 3, pp. 210-216

Intel 2007, "Open Source Computer Vision Library", last visit: http://www.intel.com/technology/computing/opencv/

Lecompte D. (2006), "Crack Detection in a Concrete Beam using Two Different Camera Techniques", Structural Health Monitoring, Vol. 5, No. 1, pp. 59-68

Lee B.J., Lee H.D. (2004), "Position-invariant neural network for digital pavement crack analysis", Computer-Aided Civil and Infrastructure Engineering Volume 19, Issue 2, pp. 105– 118.

Lee S., Chang L.M. and Chen P.H., (2005), "Performance comparison of bridge coating defect recognition methods", Corrosion 61 (2005) (1), pp. 12–20.

Lee S., Chang L.M., and Skibniewski M., (2006), “Automated recognition of surface defects using digital color image processing”, Automation in Construction, Vol 15, Issue 4, pp. 540-549

Malik J. and Perona P. (1990), "Presattentive texture discrimination with early visual mechanisms", J. Opt. Soc. America 7A(5), pp. 923-932

Ohio Department of Natural Resources (ODNR), (1999), “Dam Safety: Problems with Concrete Materials”, Division of Water Fact Sheet 99–56

Otsu N., (1979), “A threshold selection method from gray-scale histogram”, IEEE Trans. Syst. Man Cybern. 9 (1), pp. 62–66.

Patterson A.M., Dowling G.R., and Chamberlain D.A., (1997), “Building Inspection: Can Computer Vision Help”, Automation in Construction,

Portland Cement Association (PCA), 2006, last visit: http://www.cement.org/decorative/arch_panels.asp

Portland Cement Association (PCA), 2007a, “Concrete Basics”, last visit: http://www.cement.org/basics/concretebasics_concretebasics.asp

Portland Cement Association (PCA), 2007b, “Concrete Construction”, last visit: http://www.cement.org/tech/cct_con_design_bugholes.asp

Prine D. W., (1995), “Problems Associated with Nondestructive Assessment of Bridges”, SPIE Conference on Nondestructive Assessment of Aging Bridges and Highways, Oakland, CA, June 6-7, 1995

Pynn J.; Wright A.; Lodge R., (1999), “Automatic identification of cracks in road surfaces”, Image Processing and Its Applications, 1999. Seventh International Conference on (Conf. Publ. No. 465), Volume 2, pp. 671 - 675

Sinha S.K. and Fieguth P.W. (2006), “Automated detection of cracks in buried concrete pipe images”, Automation in Construction, Volume 15, Issue 1, 2006.

Sitar M., (2005), “A maintenance strategy based on prevention, inspection and detection keeps facilities operating safely and cost-effectively”, Maintenance Solutions October 2005 Issue, last visit: http://www.facilitiesnet.com/ms/article.asp?id=3455&keywords=concrete,%20flooring,%20floor%20maintenance,%20concrete%20maintenance

Starnes M. A., Carino N. J., and Kausel E. A., (2003), “Preliminary Thermography Studies for Quality Control of Concrete Structures Strengthened with Fiber-Reinforced Polymer Composites”, J. Mat. in Civ. Engrg., Volume 15, Issue 3, pp. 266-273, May/June 2003

Suwwanakarn S., Zhu Z. and Brilakis I. (2007) "Automated Air Pockets Detection for Architectural Concrete Inspection", ASCE Construction Research Congress, 6-8 May 2007, Freeport, Bahamas

Tommy Y, Lo K.T.W, and Choi, (2004), “Building defects diagnosis by infrared thermography”, Journal of Structure Survey, Volume 22, Issue 5 pp. 259-263.

Tung PC., Hwang YR., Wu MC., (2006), “The development of a mobile manipulator imaging system for bridge crack inspection”, Automation in Construction, Vol. 1, Issue 6, pp. 717 – 729.

Wilson M.L., (2006), “Concrete troubleshooting”, presented at the International Building Show, last visit: http://www.buildersshow.com

Yitzhaky Y. and Peli E. (2003). "A method for objective edge detection evaluation and detector parameter selection.", IEEE Trans. Pattern Anal. Mact. Intell., 25(8), pp. 1027-1033

Yu SN., Jang JH., and Han CS, (2007), “Auto inspection system using a mobile robot for detecting concrete cracks in a tunnel”, Automation in Construction, Vol 16, Issue 3, pp 255-261

Zou Y. and Dunsmuir W.T.M., (1997), “Generalized max/median filtering”, Proc. of Intern. Conference on Image Processing, U.S.A., IEEE Signal Processing Society, IEEE International Conference on Image Processing, Oct 26-29 1997 pp 428 – 431.